ACS Biomaterials SCIENCE & ENGINEERING

pubs.acs.org/journal/abseba

Article

Polyplex-Loaded Hydrogels for Local Gene Delivery to Human Dermal Fibroblasts

Jose Antonio Duran Mota, Júlia Quintanas Yani, Benjamin D. Almquist, Salvador Borrós,* and Nuria Oliva*

Cite This: https://doi.org/10.1021/acsbiomaterials.1c00159

Read Online

ACCESS | Metrics & More | Article Recommendations | Supporting Information

ABSTRACT: Impaired cutaneous healing leading to chronic wounds affects between 2 and 6% of the total population in most developed countries and it places a substantial burden on healthcare budgets. Current treatments involving antibiotic dressings and mechanical debridement are often not effective, causing severe pain, emotional distress, and social isolation in patients for years or even decades, ultimately resulting in limb amputation. Alternatively, gene therapy (such as mRNA therapies) has emerged as a viable option to promote wound healing through modulation of gene expression. However, protecting the genetic cargo from degradation and efficient transfection into primary cells remain significant challenges in the push to clinical translation. Another limiting aspect of current therapies is the lack of sustained release of drugs to match the therapeutic window. Herein, we have developed an injectable, biodegradable, and cytocompatible hydrogel-based wound dressing that delivers poly(β-amino ester)s (pBAEs) nanoparticles in a sustained manner over a range of therapeutic windows. We also demonstrate that pBAE nanoparticles, successfully used in previous in vivo studies, protect the mRNA load and efficiently transfect human dermal fibroblasts upon sustained release from the hydrogel wound dressing. This prototype wound dressing technology can enable the development of novel gene therapies for the treatment of chronic wounds.

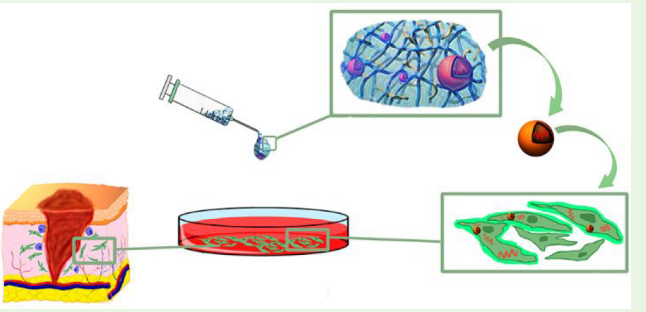

KEYWORDS: *hydrogel, polyethylene glycol, poly(β-amino ester)s, nanoparticles, gene delivery, human dermal fibroblasts, skin, wound healing*

INTRODUCTION

Wound healing is a complex process involving four highly orchestrated phases.[1,2] Failure to complete these normal stages in a coordinated fashion leads to impaired cutaneous healing, such as delayed acute wounds and chronic wounds.[3] In the United States alone, more than 6 million people suffer from chronic wounds, typically due to underlying conditions like obesity, diabetes, or ischemia. In 2014, wound care products accounted for $2.8 billion of the global healthcare budget, and by 2024, the advanced wound care market for surgical wounds and chronic ulcers is expected to exceed $22 billion.[4] Current clinical approaches to chronic wound care are quite limited given the societal impact and consist of approaches such as antibiotic dressings, mechanical debridement and offloading, and negative pressure therapy. When these treatments fail to work for wounds such as diabetic ulcers, many times, amputation becomes necessary.[5−8]

Impaired wound healing has been associated with alterations in the expression of genes that mediate healing,[9−11] positioning mRNA delivery as an attractive therapeutic approach to restore normal protein expression and promote healing.[12] mRNA therapies can also be exploited to promote cells to synthesize therapeutic proteins efficiently and safely.[13,14] However, the delivery of nucleic acids is challenging, because of their susceptibility to rapid degradation, clearance in biological fluids, and inability to cross cytoplasmatic membranes.[15] Numerous vehicles have been developed over the past decade, each with its own limitations and challenges.[15,16] For example, viral vectors are capable of high transduction efficiency and sustained transgene expression, but they cause high levels of immunogenicity, limiting their translation to human use.[17] In contrast, nonviral vectors show lower transfection efficiencies than viruses, but are usually cheaper to synthesize, present better loading capacities for both DNA and RNA, and are safer for the host.

Cationic polymers, such as poly(β-amino ester)s (pBAEs), are a type of nonviral vector able to neutralize negatively

Special Issue: Advanced Biomedical Hydrogels

Received: January 31, 2021
Accepted: May 21, 2021

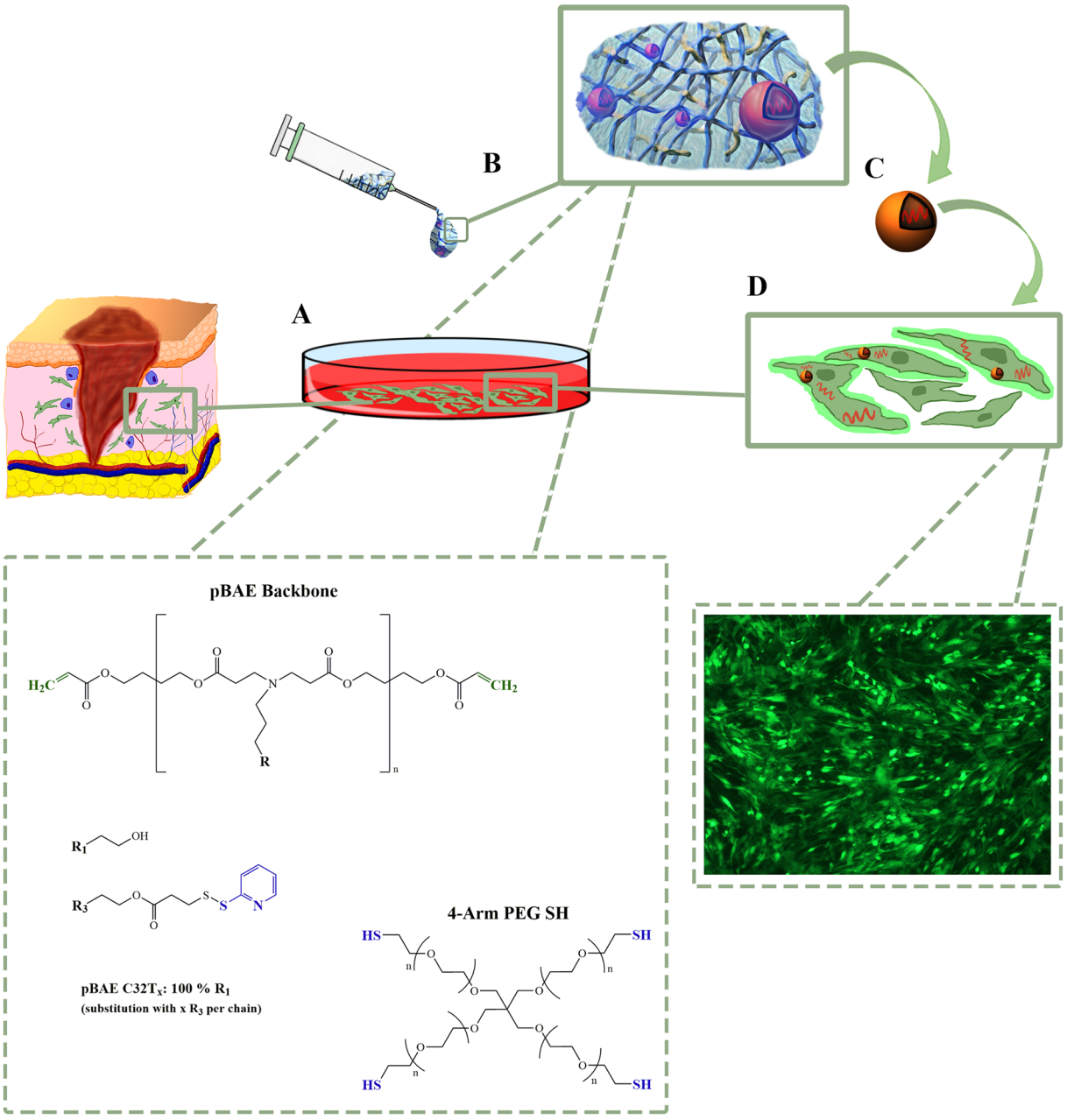

Figure 1. Schematic diagram of the composite hydrogel wound dressing designed herein for applications involving human dermal fibroblasts transfection, based on a pBAE-PEG injectable hydrogel doped with mRNA-loaded polyplexes. (A) Human dermal fibroblast culture. (B) pBAE-PEG hydrogel containing gene-loaded pBAE polyplexes. (C) Release of pBAE nanoparticles. (D) Human dermal fibroblasts transfected using mRNA-GFP-loaded pBAE polyplexes.

charged oligonucleotides and form discrete particles, also known as polyplexes, through electrostatic interactions.[18−23] Polyplexes' positive overall net charge allows them to bind to cell membranes and enter the cytoplasm via endosomal transport. In addition, amines and terminal acrylates in these polymers confer the versatility of incorporating chemical groups into their structure to tune their functions and properties,[21,24] such as improving transfection efficiencies by conjugating endosomolytic moieties.[25] Moreover, pBAEs are biodegradable and biocompatible.[26] In recent years, we have developed many oligopeptide-modified pBAEs polyplexes (OM-pBAEs),[21,27] showing high transfection efficiency and excellent biocompatibility in different cancer cell lines,[22,28−30] as well as efficient in vivo transfection,[31] making these nanoparticles a highly promising candidate for clinical translation of new cancer therapies. However, efficient transfection of primary human cells remains a challenge,[32−35] hampering the progress of new gene therapies for numerous noncancerous pathologies, such as chronic wounds.

Local delivery of therapeutics, and particularly nucleic acids[36] is often preferred over systemic delivery, as it allows for reduced dosages, enhanced stability, and increased biocompatibility.[37] Moreover, the smart design of local delivery platforms allows for sustained and controlled release of therapeutics to injured or diseased cells, a critically important aspect in the highly dynamic process of wound

https://doi.org/10.1021/acsbiomaterials.1c00159
ACS Biomater. Sci. Eng. XXXX, XXX, XXX−XXX

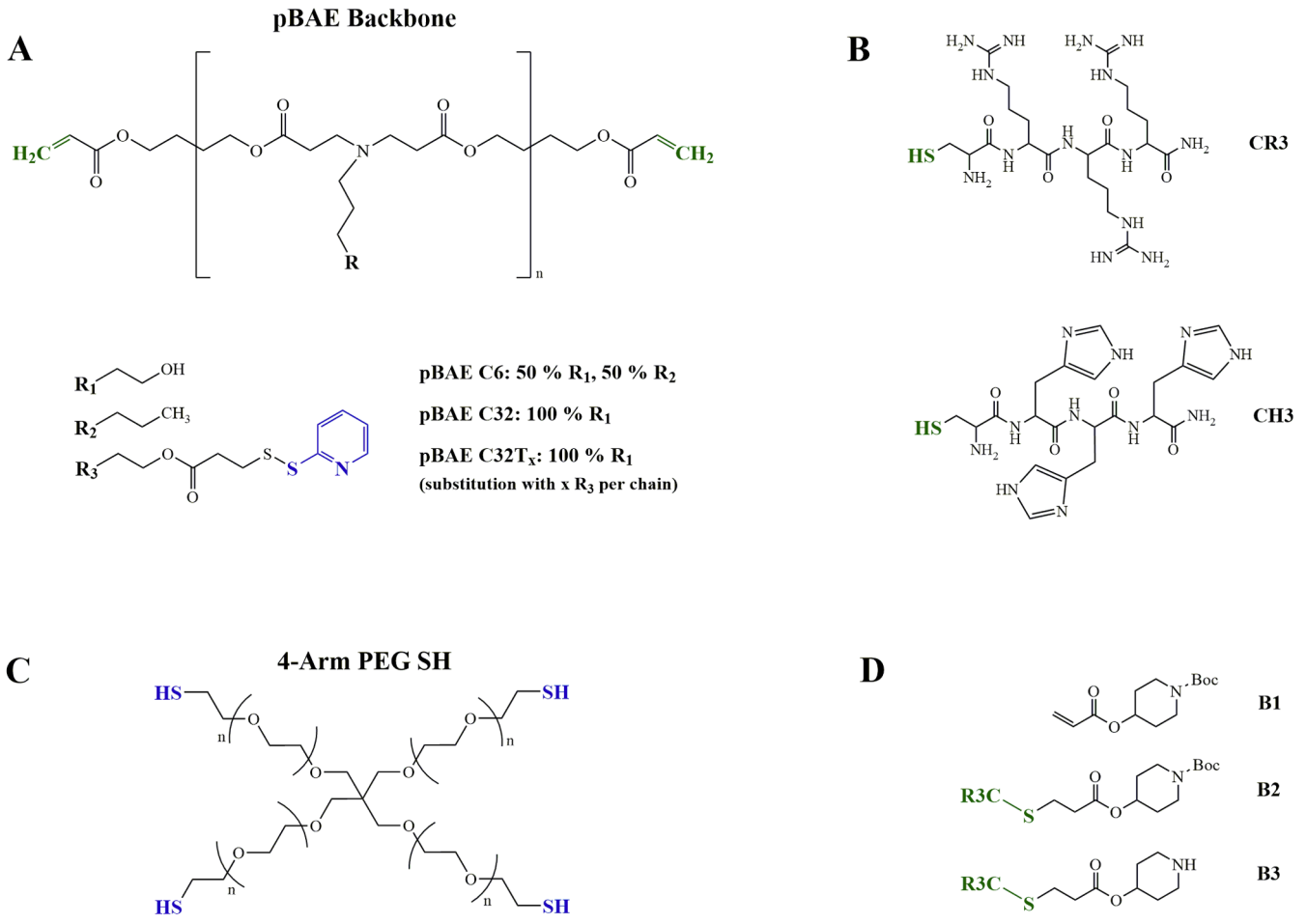

Figure 2. (A) General chemical structure of pBAE polymers, where the ratio and chemical identity of R (R1, alkyl alcohol; R2, alkyl; or R3, thiopyridyl ester) define the nomenclature of the final product (C6, C32, or C32T$_x$). (B) Chemical structure of arginine (CR3) and histidine (CH3) oligopeptides used to modify the terminal acrylates of pBAE polymers. (C) Chemical structure of 4-arm PEG-SH used to cross-link C32T$_x$ polymers to form the hydrogel network. (D) Protecting groups used during the synthesis of the various pBAE custom polymers.

healing.[38,39] The structure and properties of hydrogels make them optimal candidates to release therapeutic nanoparticles for wound healing,[40−42] maintaining a warm moist environment and allowing the absorption of wound exudates and adequate oxygen circulation, necessary to promote healing and prevent bacterial infections.[43,44] Moreover, hydrogels' hydrophilic nature, capable of absorbing up to 90% of water or fluids, confers them high porosity and mechanical properties resembling those of human tissues. Other characteristics such as biodegradability, biocompatibility, low immunogenicity, and ease of usage have propelled their translation to the clinic.[45]

In the present work, we describe and characterize a new local gene delivery platform for cutaneous wound healing based on a composite synthetic hydrogel, made of pBAE and PEG polymers, doped with polynucleotide-loaded pBAE nanoparticles (Figure 1) to enable efficient transfection of human dermal fibroblasts (HDFs). Efficient transfection of HDFs is essential for developing new gene therapies for wound healing owing to their extensive involvement in the process of wound healing,[7,46] and their reported altered gene expression profile in chronic wounds.[47−50] The hydrogel developed herein is injectable, enabling in situ polymerization and high surface contact area in deep wounds with irregular topography, a typical feature of chronic wounds like diabetic foot ulcers. In the future, the versatility of pBAEs will allow for further modifications of the hydrogel network and/or the polyplexes to incorporate new and improved features to this novel wound dressing platform, such as smarter control over the release or tissue- and cell-specific transfection.

MATERIALS AND METHODS

Materials. Reagents and solvents were purchased from Sigma−Aldrich and Panreac and used as received unless otherwise stated. Oligopeptides were obtained from Ontores Biotechnologies Inc. Plasmid reporter green fluorescent protein (pmaxGFP) (3486 bp) was acquired from Amaxa, CleanCap EGFP mRNA (5moU) from Tebu-Bio, Firefly Luciferase reporter plasmid FLuc from Promega Corporation, and CleanCap Fluc mRNA 5-methoxyuridine from TriLink. Human dermal fibroblasts (HDFs) from adult skin were purchased from ATCC (ATCC PCS-201−030). Products for cell culture (DMEM, phosphate-buffered saline (PBS), glutamine and penicillin−streptomycin solution, trypsin-EDTA 0.25%) were obtained from Gibco, Hyclone, and Invitrogen. ^{1}H NMR spectra were recorded in a 400 MHz Varian (Varian NMR Instruments, Claredon Hills, IL, USA) and methanol-d$_4$ was used as solvent unless otherwise stated.

Synthesis of pBAE Polymer Backbones. Acrylate-terminated poly(β-aminoester)s C32 and C6 (Figure 2A) were synthesized following a procedure previously described in the literature by Dosta et al.[27] Specifically, the polymer formation occurs by addition reaction of primary amines with diacrylates. C32 polymer was obtained by stirring 5-amino-1-pentanol (7.7 g, 75 mmol) and 1,4-butanediol

https://doi.org/10.1021/acsbiomaterials.1c00159
ACS Biomater. Sci. Eng. XXXX, XXX, XXX−XXX

diacrylate (18 g, 82 mmol) together at 90 °C for 20 h. For C6 polymer, 5-amino-1-pentanol (3.9 g, 38 mmol) was first mixed with 1-hexylamine (3.8 g, 38 mmol). Then, 1,4-butanediol diacrylate (18 g, 82 mmol) was added to the mixture and heated at 90 °C for 20 h. Polymer backbones were characterized by ^{1}H NMR as described in our previous works,[21,31,51,52] and the number of repeated units of the polymer was confirmed to be n = 7.

Synthesis of Acrylate-Ended, Thiol-Reactive PBAE C32T$_x$. The aim is to modify the acrylate-ended C32 polymer with the group 3-(2-pyridyldithio)propanoic acid (SPDP) in order to obtain a thiol-reactive C32 pBAE (Figure 2A). To prepare the SPDP acid, the first step consisted of dissolving Aldrithiol-2 (1 g, 4.46 mmol) in ethanol. The solution was purged with argon and protected from light along the process. Glacial acetic acid was added dropwise (0.134 mL) while stirring. Finally, 3-mercaptopropionic acid (0.237 g, 2.23 mmol) was mixed with the previous solution. The flask was allowed to react for 2 h at room temperature and the final product was purified by column chromatography using basic activated Al_2O_3 as stationary phase and CH_2Cl_2:CH_3CH_2OH:CH_3COOH (60:40:1) solution as mobile phase. The incorporation of SPDP groups to C32 chains is produced via Steglich esterification. In the present work, C32T$_2$ was used. The subscript in T indicates the number of SPDP groups in a typical chain of seven monomer repetitions in average. Briefly, C32 PBAE (1 g, 0.4 mmol), SPDP (0.215 g, 1.0 mmol) and a few milligrams of 4-dimethylaminopyridine (DMAP) were dissolved in anhydrous CH_2Cl_2. The solution was cooled at 4 °C for 30 min and then N,N′-dicyclohexylcarbodiimide (DCC) (0.250 g, 1.2 mmol) was added. The mixture was allowed to react overnight at room temperature under an inert atmosphere and protected from light. Finally, the product was dissolved in acetonitrile:ethyl acetate (1:1) and kept 3 h at 4 °C to precipitate and separate DCC salts. C32T$_2$ polymer was characterized by ^{1}H NMR. The number of SPDPs per chain was confirmed by comparing integrals of signals in terminal acrylates at δ = 5.8−6.4 ppm and in thiopyridyl group at δ = 7.0−8.5 ppm (Figure S1).

Modification of Acrylate-Ended pBAEs with Oligopeptides. Peptides were purchased as trifluoroacetic acid salts. The first step was the substitution of trifluoroacetic acid for hydrochloride as counter-ions. Generally, oligopeptides (100 mg) were dissolved in HCl 0.1 M (10 mL) and frozen at −80 °C for an hour. The solution was then freeze-dried. Oligopeptides used in the present work were Cys-Arg-Arg-Arg (CR3) and Cys-His-His-His (CH3) (Figure 2B). Peptides hydrochlorides were reacted with acrylate-ended C32 or C6 polymers following a Michael-type addition at a pBAE:peptide molar ratio of 1:2.5. PBAEs and peptides were dissolved separately in dimethyl sulfoxide (DMSO) at 100 mg/mL concentration. The polymer solution was then added dropwise to the peptide solution. At this point, triethylamine was added to the solution in a peptide:triethylamine molar ratio of 1:8. The mixture was allowed to react at room temperature for 48 h. The modification of C32T$_2$ to obtain C32T$_2$CR3 polymer followed another synthetic process to prevent cysteine reaction with SPDP groups in the backbone. Shortly, thiols from oligopeptides were protected with a piperidine-derived group. First, 1-Boc-4-hydroxypiperidine (100 mg, 0.50 mmol) and triethylamine (0.115 mL, 0.80 mmol) were dissolved in CH_2Cl_2 and cooled to 0 °C. Acryloyl chloride (0.044 mL, 0.52 mmol) was added to the mixture. The solution was stirred overnight at room temperature. The product obtained (B1) was washed in a separating funnel, first with water and then with a saturated solution of sodium bicarbonate. Finally, the product B1 was dried under a vacuum (Figure 2D). In the second step, B1 (90 mg, 0.24 mmol) and the CR3 peptide (200 mg, 0.33 mmol) were dissolved separately in 0.5 mL of DMSO and then mixed. The solution was stirred overnight at room temperature. Precipitation of the product B2 (Figure 2D) occurs after adding the mixture dropwise to a solution of diethyl ether:acetone (4:1) and centrifuging at 4000 rpm for 10 min. The final step consisted of the removal of the Boc group. B2 (100 mg, 0.110 mmol) was dissolved in a solution of TFA (0.483 mL) and CH_2Cl_2 (0.887 mL). The mixture was stirred at room temperature for 4 h. The product obtained was then dried under vacuum, dissolved in a solution of CH_2Cl_2:CH_3OH (5:1), and passed through an Amberlyst A21 column. Immediately, B3 product was used to react with C32T$_2$ in a polymer:B3 molar ratio of 1:2.5, without addition of triethylamine. All OM-pBAEs were characterized by ^{1}H NMR as described in our previous works.[21,31,51,52]

PBAE Polyplex Preparation. Oligopeptide-modifiedC6 and C32 pBAE nanoparticles were prepared following protocols based on our previous works.[21,27,52] Polymers used were C6CR3, C6RH (C6CR3:C6CH3 in a 6:4 ratio), and C32CR3. Polynucleotides used in transfections were plasmid reporter green fluorescent protein (pGFP), EGFP mRNA (mRNA-GFP), firefly luciferase reporter plasmid (pFLuc), and mRNA-FLuc. PBAEs and polynucleotides were kept in stock solution at 100 mg/mL in DMSO or 1 mg/mL in nuclease-free water, respectively. For polyplexes formation, these starting solutions were diluted separately in sodium acetate (AcONa) pH 5.2 buffer. The concentration of AcONa salts used was 12.5 mM for C6 or 25 mM for C32. The final volume of the pBAE and the polynucleotide solutions was the same and it was calculated to reach a polynucleotide final concentration of 0.03 mg/mL and the desired pBAEs:polynucleotide weight ratio when mixed. This ratio was 25:1 for C6 and 50:1 for C32. In relation to the mixing process, the polynucleotide solution was added over the PBAE solution by pipetting and incubating at 25 °C for 30 min. Analysis of particle size distribution was performed in a Nanosizer ZS instrument (Malvern Instruments, UK) diluting polyplexes in a 10-fold volume of phosphate-buffered saline (PBS 1×).

Preparation of PEG-pBAE Hydrogels. Hydrogel matrix formation occurs by the cross-linking of 4arm-PEG-SH molecules (M_n = 5000) with C32T$_2$CR3 pBAE (Figure 2C) in different PEG:pBAE ratios. The presence of SPDP in the C32T$_2$CR3 polymer allows the chemical cross-linking with thiols in the PEG polymer, hence forming the hydrogel in situ. For its preparation, the 4arm-PEG-SH and C32T$_2$CR3 were separately dissolved in DMSO at a concentration of 500 and 250 mg/mL, respectively. The pBAE solution was added over the PEG solution to achieve the desired PEG:pBAE ratio after mixing. The solution was mildly shaken and incubated at room temperature for 30 min. Finally, each sample was washed with deionized water five times to fully eliminate DMSO traces. Hydrogels used in the present work had PEG:pBAE molecule ratios of 1:1 (HG11, one PEG is cross-linked with one linear C32T$_2$CR3) and 1:4 (HG14, a PEG molecule is cross-linked using four C32T$_2$CR3 pBAE).

Preparation of PEG-pBAE Hydrogels Doped with pBAE Nanoparticles. Following the pBAE Polyplex Preparation section detailed above, we prepared 4 μL of pBAE nanoparticle solution at a 0.3 mg/mL polynucleotide concentration. Before forming the hydrogels, nanoparticle solutions were first mixed with the PEG solution. PBAE solution was then added to the mixture and the Preparation of PEG-pBAE Hydrogels protocol described above was followed without changes. To further understand the hydrogel behavior, we prepared the two formulations studied in the present work with or without nanoparticles and using different concentrations and final volumes (Table 1).

Confocal Microscopy Characterization of PEG-pBAE Hydrogels. Microstructure of hydrogels and polyplex-loaded hydrogels were studied by confocal fluorescence microscopy. For pore size and distribution studies, we prepared the hydrogels using 0.5% of the C32T$_2$CR3 polymer forming the hydrogel matrix tagged with fluorescein isothiocyanate (FITC). Hydrogels were immersed in an optimal cutting temperature (OCT) compound and frozen at −80 °C overnight and then 25 and 50 μm thickness slices were obtained with a cryotome. For studies of polyplex distribution, hydrogels loaded with pBAE nanoparticles were prepared following the protocol described in the previous section. Specifically, pGFP-loaded C6RH polyplexes were embedded inside the hydrogels, where 2% of C6RH polymer was labeled with cy5 dye and 10% of pGFP was labeled with cy3 dye to image both the nanoparticle and the polynucleotide cargo and study dye colocalization as a surrogate for nanoparticle stability in the hydrogel structure. Hydrogels were immersed in distilled water for 30 min to wash nanoparticles that may be weakly adsorbed on the

https://doi.org/10.1021/acsbiomaterials.1c00159
ACS Biomater. Sci. Eng. XXXX, XXX, XXX−XXX

Table 1. Summary of Initial Concentrations, Volumes, and Final Volumes of the Different Hydrogel Formulations Studied in the Present Work[a]

formulation	$[PEG]_i$	V_{PEG}	$[pBAE]_i$	V_{pBAE}	V_{NP}	V_{DMSO}	V_f
HG11	500	8	250	8	0	0	16
HG14	500	8	250	32	0	0	40
HG11-NP	500	8	250	8	4	0	20
HG14-NP	500	8	250	32	4	0	44
HG14-NP$_{1/2}$	500	8	250	32	2	2	44
HG11−S00v	500	8	500	4	0	12	24
HG14−S00v	500	8	500	16	0	0	24
HG11-NP-S00v	500	8	500	4	4	12	28
HG14-NP-S00v	500	8	500	16	4	0	28

[a]Concentration is given in mg/mL and volumes in μL.

hydrogel surface prior to imaging. Images were taken using a Leica SP8 confocal microscope (Leica Microsystems). Depending on the experiment, FITC, cy3, and cy5 wavelengths were selected using the microscope software. Image processing, pore size distribution, analysis, and colocalization studies were done with *ImageJ-Fiji* software.

Sample Preparation for Scanning Electron Microscopy (SEM). Hydrogel formulations with and without nanoparticles were prepared following the protocol described in the previous section. Samples were frozen at −80 °C overnight and freeze-dried prior to imaging with a SEM. No sputter coating was used for the visualization of the samples.

Hydrogel Swelling. Duplicate of samples HG11 and HG14 were prepared following the protocol given above. Different drying processes were followed in parallel to compare hydrogel behavior. In the first method, samples were dried for 24 h in a lab oven at 37 °C. Alternatively, samples were frozen at −80 °C overnight and a lyophilized afterward. The residue obtained after each drying method was weighted. Hydrogels were then incubated in 1 mL of Milli-Q water for 30 min. Throughout the process, the samples were slightly squeezed with tweezers to facilitate the complete entry of water into the networks. Swollen hydrogels were weighted and then the swelling ratio was calculated with the following equation:

$$\text{swelling}(\%) = \frac{W_s - W_d}{W_d} 100 \quad (1)$$

Where W_s and W_d refer to the weight of the swollen hydrogel and the dried hydrogel, respectively.

Hydrogel Rheological Characterization. Triplicates of samples of HG11and HG14 were freshly prepared and immediately used in the measurements. Storage (G') and loss (G'') moduli were measured as a function of the strain at 25 °C with Ar2000ex rheometer (TA Instruments) using 8 mm Cross-Hatched plate. A different gap was set depending on the sample, but always setting a normal force of 0.1 N.

Hydrogels Degradation Times. Hydrogels HG11 and HG14were prepared following the protocol described previously, and $C32T_2CR3$ was tagged with fluorescein at a concentration of 2.5% (w/w) for HG11 and 5% (w/w) for HG14. Duplicates of these candidates were incubated at 37 °C in 200 μL PBS (1×). The supernatant (200 μL) was completely removed to measure fluorescence intensity at each time point and replaced with the same volume of fresh PBS solution. The progression of the degradation was followed by tracking fluorescence loss with plate and cuvette reader Tecan Infinite 200 PRO. The percentage of hydrogel integrity was calculated on the basis of the fluorescence intensity in each time point relative to the total fluorescence.

PBAE Nanoparticle Release. Duplicate samples of HG11 and HG14 doped with C6RH pBAE nanoparticles were prepared. These polyplexes contained pGFP labeled with cy5. Samples were placed in PBS (1x) and at each time point the supernatant (200 μL) was collected to measure fluorescence intensity and the same volume was replaced with fresh PBS solution. Nanoparticle release from the hydrogel was followed by tracking fluorescence loss. The percentage of released nanoparticles was calculated on the basis of the fluorescence intensity in each time point relative to the total fluorescence.

HDFs Cell Culture. HDF cell line was cultured with DMEM (4.5 g glucose/mL, without glutamine, pH = 7.2) supplemented with glutamine (2 mM), 1% penicillin−streptomycin mixture and 10% fetal bovine serum (FBS). Cells were grown on incubators at 37 °C with a 5% CO_2 atmosphere and seeded 72 h before starting an experiment. HDF cells used in every experiment were at passage number 2.

Cytotoxicity of Hydrogel Degradation Products. Triplicate samples of HG11 and HG14 hydrogels were degraded in a milliliter of supplemented culture medium without FBS and incubated at 37 °C. Three aliquots of 200 μL of each sample were collected at 24, 72, and 168 h and replaced with fresh medium. The starting reagents used to form the hydrogels were also dissolved separately in culture medium in a quantity corresponding that used for the hydrogel preparation. Before use, 10% FBS was added to each sample. HDF cells were seeded at a density of 10 000 cells per well in a 96-well plate and were grown in contact with the collected 200 μL medium containing the hydrogel degradation products or the starting reagents. Cell viability assays were performed at 24 h using Presto Blue reagent (Invitrogen) following the manufacturer's instructions. Briefly, presto blue reagent was added and incubated for 30 min at 37 °C. Fluorescence intensity was measured then at 540 nm excitation and 590 nm emission wavelengths.

HDFs Transfection with pBAE Nanoparticles. HDF cells were seeded at 10 000 cells per well in 96-well plates and incubated for 24 h at 37 °C in 5% CO_2 atmosphere. Cells reached a confluence of 80−90% prior to performing the transfection experiments. Different compositions of pBAE nanoparticles loaded with pGFP, pFLuc, mRNA-GFP, and mRNA-FLuc polynucleotides were studied in the transfection experiments. Solutions of these polyplexes were prepared in a concentration of 0.03 μg/μL as described above and 10-fold diluted in nonsupplemented DMEM. Cells were transfected with 100 μL of the previous solution to a final 0.3 μg/well dose of the polynucleotide. HDFs were incubated for 3 h. Subsequently, transfection media was removed, and fresh supplemented media was added to the cells. Polyplus-transfection JetPrime and Jet-MESSENGER were used as positive control in DNA and RNA experiments, respectively. The concentration used was that recommended by the manufacturer, which corresponds to a lower concentration than that used for pBAE nanoparticles due to the toxicity of JetPrime and JetMESSENGER. Untreated cells were used as negative controls. After 24 h of incubation in the case of mRNA and 48 h for plasmid DNA, cells were imaged with a fluorescence microscope (Nikon Eclipse T32000-U). For quantitative measurements, cells were detached by incubating for 5 min with trypsin-ethylenediaminetetraacetic acid at 37 °C in 5% CO_2 atmosphere. Transfection efficiency was measured by flow cytometry (FACS; NovoCyte Flow Cytometer, ACEA Biosciences Inc.). In case of using FLuc reporters, luciferase activity was quantified using the Luciferase Assay System Kit (Promega), and photon emission was measured in a Synergy HT luminometer (BioTek). Cell viability of the formulations studied was performed using Presto Blue reagent and following the manufacturer's instructions. Negative control consisted of untreated cells and positive control consisted of cells transfected using the Polyplus reagent.

HDF Transfection with Hydrogel Doped with pBAE Nanoparticles. HDF cells were seeded at 40 000 cells per well in 48-well plates and incubated 24 h at 37 °C in a 5% CO_2 atmosphere. Triplicate samples of HG41 and HG44 containing mRNA-GFP-loaded C6RH pBAE polyplexes were prepared as described above. Hydrogels were washed with supplemented DMEM five times to eliminate DMSO traces and placed on top of cells together with 250 μL of supplemented medium. Negative control consisted of the same hydrogels incorporating C6RH loaded with noncoding DNA segments. After 24 h of incubation, cells were imaged with a fluorescence microscope. Transfection efficiency was measured

https://doi.org/10.1021/acsbiomaterials.1c00159
ACS Biomater. Sci. Eng. XXXX, XXX, XXX−XXX

A

Nanoparticle formulation	Hydrodynamic diameter (nm; by DLS)	PdI (by DLS)	Z-Potential (mV; by DLS)
C32CR3	187 ± 14	0.12 ± 0.03	35 ± 2
C6CR3	132 ± 4	0.20 ± 0.02	30 ± 1
C6RH	127 ± 1	0.15 ± 0.01	30 ± 1

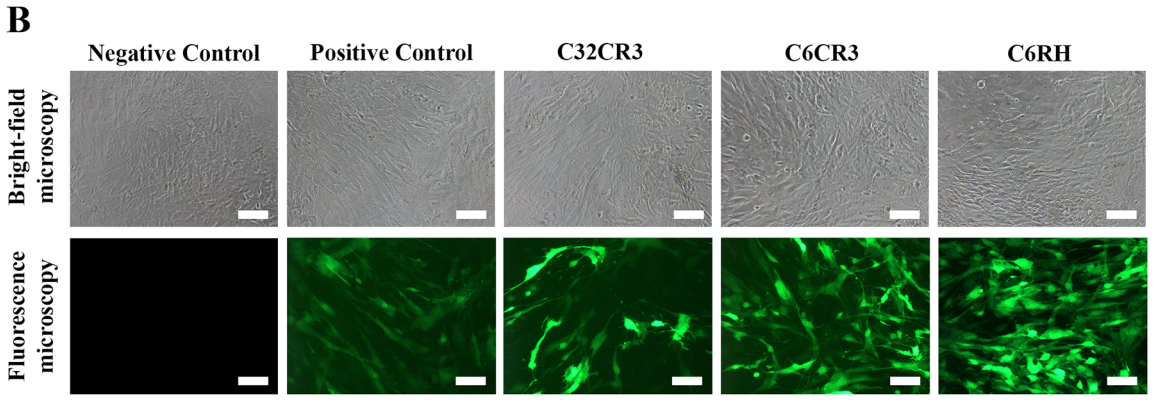

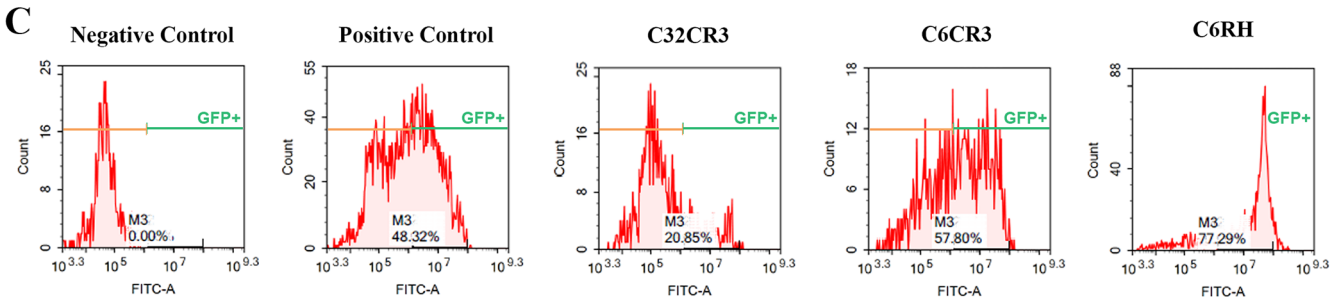

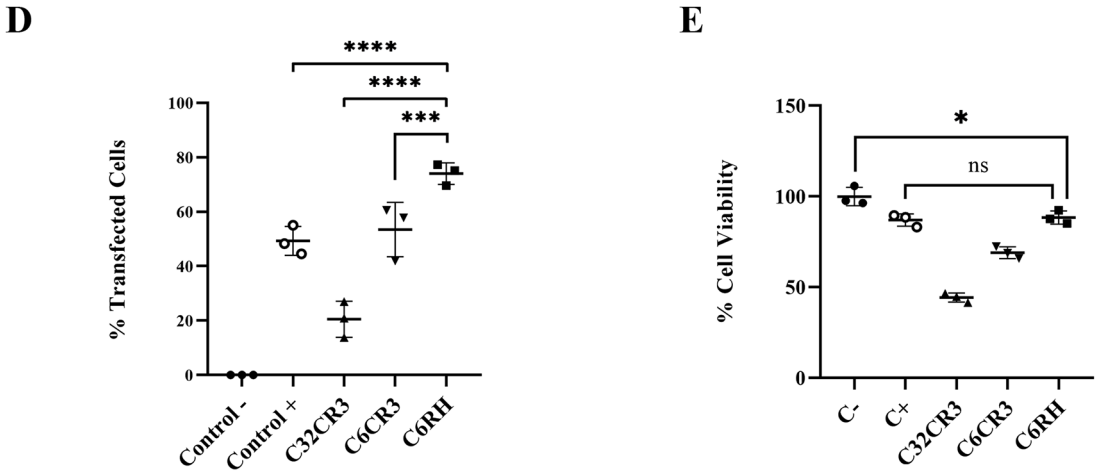

Figure 3. (A) Hydrodynamic diameter, PdI and Z-potential of the different pBAE formulations (C32CR3, C6CR3, or C6RH) containing GFP-coding mRNA obtained by DLS technique. (B) Bright-field and fluorescence microscopy images of HDF cell line expressing GFP after transfection with commercially available jetMESSENGER or different pBAE formulations containing mRNA. (C) FACS graphs showing the percentage of the events counted emitting radiation at FITC wavelength. (D) Quantification of transfected cells (in %) by FACS with the different formulations encapsulating GFP-coding mRNA. Imaging and quantification assays were performed 24 h after transfection. (E) Cell viability (in %) after 24 h transfection using the mRNA-GFP-loaded polyplexes formulations studied. Scale bar: 100 μm. $n = 3$. *$p < 0.05$; **$p < 0.01$; ***$p < 0.001$; ****$p < 0.0001$.

afterward by flow cytometry in the same conditions as mentioned in the previous section. A positive control consisting of the formulation HG11 loaded with Polyplus JetMESSENGER polyplexes was used. The protocol from the manufacturer was adapted to meet the same mRNA quantity incorporated into the hydrogel. A cell viability assay was performed after 24 h of treatment with the formulations studied

https://doi.org/10.1021/acsbiomaterials.1c00159
ACS Biomater. Sci. Eng. XXXX, XXX, XXX−XXX

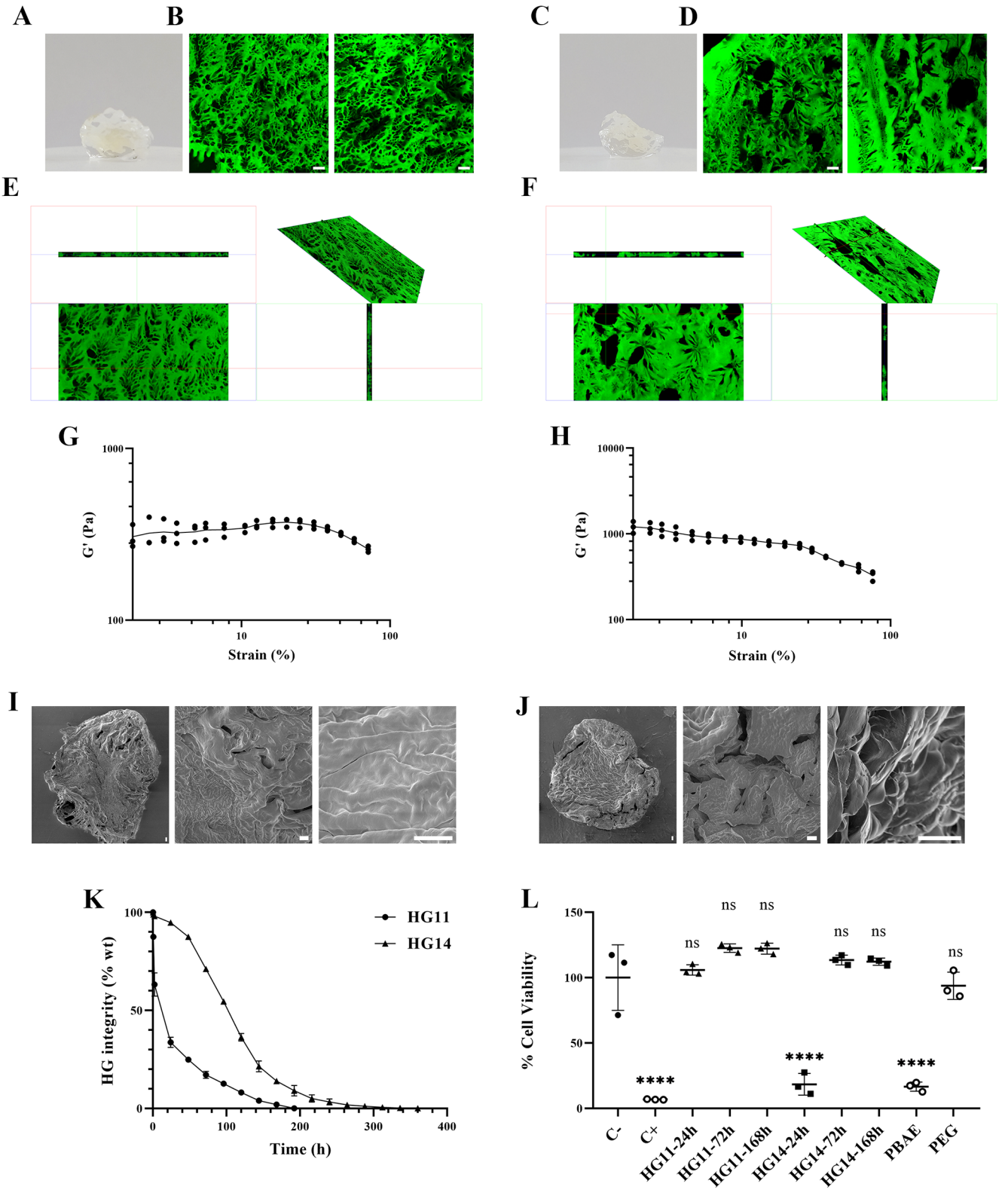

Figure 4. (A) Image of hydrogel formulation HG11. (B) Confocal microscopy images of 50 μm thickness slices from the HG11 hydrogel tagged with FITC. (C) Image of hydrogel formulation HG14. (D) Confocal microscopy images of 50 μm thickness slices from the HG14 hydrogel tagged with FITC. (E, F) 3D reconstruction of formulations HG11 and HG14, respectively. (G, H) G′-strain curve for HG11 and HG14 hydrogel formulations, respectively; n = 3. (I, J) SEM images (SEM HV: 1 kV) of bulk lyophilized HG11 and HG14, respectively. (K) Degradation of hydrogels HG11 and HG14 was tracked using fluorescently labeled pBAE, which was converted to weight% of pBAE in the hydrogel as a measure of hydrogel integrity; n = 2. (L) Viability of HDFs after 24 h in contact with medium containing the degradation byproducts released from the hydrogels during three time intervals (0−24 h, 24−72 h, and 72−168 h). Confocal microscopy images scale bar: 100 μm; SEM scale bar: 50 μm. n = 3. *p < 0.05; **p < 0.01; ***p < 0.001; ****p < 0.0001.

https://doi.org/10.1021/acsbiomaterials.1c00159
ACS Biomater. Sci. Eng. XXXX, XXX, XXX−XXX

using Presto Blue reagent and following the manufacturer's instructions. Negative control consisted of untreated cells and positive control consisted of treating cells with a highly cytotoxic solution. The cytotoxicity of the Polyplus control was also measured.

Statistical Analysis. *GraphPad Prism 8.0.1* software was used for the statistical analysis. Statistical differences between groups were studied by ordinary one-way ANOVA with posthoc Tukey HSD test. The significance of the difference in the data is $*p < 0.05$, $**p < 0.01$, $***p < 0.001$, and $****p < 0.0001$.

RESULTS AND DISCUSSION

The platform developed here consists of a cytocompatible, biodegradable, and injectable PEG:pBAE hydrogel for the local and sustained delivery of mRNA-loaded pBAE nanoparticles to transfect HDFs. We exploited the chemical versatility of pBAEs to optimize the polyplex formulation to transfect primary dermal fibroblasts. We further exploited the versatility of pBAEs by using these polymers as the hydrogel backbone that protects the nanoparticles and allows their sustained release over time.

Synthesis and Characterization of Oligopeptide End-Modified pBAEs. pBAEs present high tunability and versatility. The polymer backbone's chemical structure plays a decisive role in the formation of polyplexes and their behavior as transfection agents. In this work, we synthesized two families of pBAE polymers with varying polarity by controlling the molar stoichiometry of amine groups, with the C32 polymer being more hydrophilic than the C6 polymer (Figure 2A). To enable cross-linking of the pBAE polymers with 4arm-PEG-SH molecules, we synthesized thiol-reactive C32 pBAEs ($C32T_x$), with x being approximately two thiopyridyl groups per chain (Figure 2A, Figure S1). Finally, the different pBAE acrylate-ended backbones (C6 C32 and $C32T_2$) were modified with cysteine-terminated CR3 or CH3 oligopeptides through Michael-type addition (Figure 2B, Figure S2). All ^{1}H NMR spectra of polymers are in agreement with previously published data.[27,52]

Optimization, Characterization, and Transfection Efficiency of OM-pBAE Polyplexes. Several cancer cell lines have been successfully transfected using a wide variety of pBAE formulations.[21,27,51] However, transfection of primary human cells, such as fibroblasts, is challenging and typically yields very low transfection efficiency. We have based our current study on previously observed patterns that yielded optimal transfection efficiency in cancer cell lines, and systematically altered polyplexes formulation to tune the hydrophobicity/hydrophilicity ratio and the ability to escape the endosome, to maximize fibroblast transfection. Past research has shown that hexyl groups in polyplexes enhance endocytosis and transfection efficiency[53,54] but decrease nanoparticle stability.[27] Alternatively, the use of alcohol pendant groups combined with hydrocarbon chains overcomes the stability limitations and affords efficient transfection (C6 polymers, Figure 2A).

Regarding endosomal escape, our previous research showed that the addition of histidine residues presents the best buffering capacity despite low encapsulation of genetic material.[21] On the other hand, arginine-ended OM-pBAEs showed higher encapsulation efficiency with lower endosomal escape capacity. Polyplexes formed by a mixture of equal ratios of both polymers C32CR3 and C32CH3 (1:1) led to synergistic transfection efficiencies. Based on these studies, here we hypothesized that a mixture of arginine-ended (CR3) and histidine-ended (CH3) C6 pBAE polymers, which are more hydrophobic than previously studied C32 polymers (Figure 2B), would maximize oligonucleotide encapsulation, enable cellular membrane crossing and facilitate endosomal escape in primary HDFs.[27] Hybrid C6CR3:C6CH3 polyplexes with a 3:2 molar ratio (named C6RH from now on) showed efficient encapsulation of GFP-mRNA into nanoparticles of similar size, polydispersity index and Z-potential to its predecessors (C32CR3 and C6CR3, Figure 3A, Supplemental figure S3), previously proven to be optimal for cellular uptake[55,56] and in vivo use.[57−60] C6RH can also encapsulate other genetic material, such as plasmid DNA, and genetic material encoding other proteins, such as luciferase (Table S1). C6CH3- and C32CH3-only polyplexes were not investigated because of near-null transfection rates observed in the past.[21]

Transfection efficiency was evaluated 24 h post-transfection with GFP-mRNA polyplexes compared to controls. GFP expression in cells was observed by fluorescence microscopy (Figure 3B) before its quantification by flow cytometry (FACS, Figure 3C, D). Overall, C6RH polyplexes demonstrated superior GFP-mRNA transfection efficiency in HDFs than previously developed formulations (C32CR3 and C6CR3) and a commercially available transfection reagent (Figure 3B−D). These results suggest that by tuning the pBAE backbone's hydrophobicity and the oligopeptide modification ratios, C6RH polyplexes can cross HDFs membranes more readily and successfully escape the endosome, leading to an overall enhancement of transfection efficiency and reporter protein expression, while eliciting minimal toxicity (Figure 3E). Interestingly, the levels of plasmid DNA expression after transfection with C6RH polyplexes were also higher than those of previous formulations and a commercially available control (Figure S4), indicating that C6RH nanoparticles have an enhanced ability to cross the nuclear membrane and deliver genetic material to the nucleus, a unique feature for these polyplexes. To confirm this approach's broad applicability, we verified that these polyplexes successfully deliver mRNA and plasmid DNA encoding other proteins (such as luciferase) (Figure S5). All in all, C6RH polyplexes emerge as new candidates for future applications as gene delivery vehicles because of their versatility, high transfection efficiency, and low toxicity, and are suitable for the delivery of both DNA and RNA to primary human dermal fibroblasts.

Preparation and Characterization of PEG:PBAE Hydrogels. Following the successful development of C6RH polyplexes, we next explored incorporating them into a degradable hydrogel to facilitate localized, controlled delivery. We chose C32CR3 pBAEs to form the hydrogel's backbone due to their hydrophilicity (100% alcohol pendant groups), as well as their biodegradability and biocompatibility. C32CR3 pBAEs were chemically modified to make them thiol-reactive ($C32T_2CR3$) and star-shaped 4arm-PEG-SH was used as a cross-linker to form the hydrogel network in situ (Figure 1 and Figure 4A, C). The formation of the hydrogel network was monitored by the disappearance of the leaving group pyridine-2-thione signals in the ^{1}H NMR spectrum (Figure S6).

By controlling the PEG:pBAE ratio and cross-linking density, mechanical properties of the hydrogel can be readily tuned. We explored two PEG:pBAE molar ratios in the present work: 1:1 (HG11), where thiol groups are in 2-fold excess of thiol-reactive groups and 1:4 (HG14), with a 2-fold excess of thiol-reactive groups compared to thiol groups. We studied the impact of these different ratios on the hydrogel's properties to establish our material's optimal formulation. Interestingly, the

https://doi.org/10.1021/acsbiomaterials.1c00159
ACS Biomater. Sci. Eng. XXXX, XXX, XXX−XXX

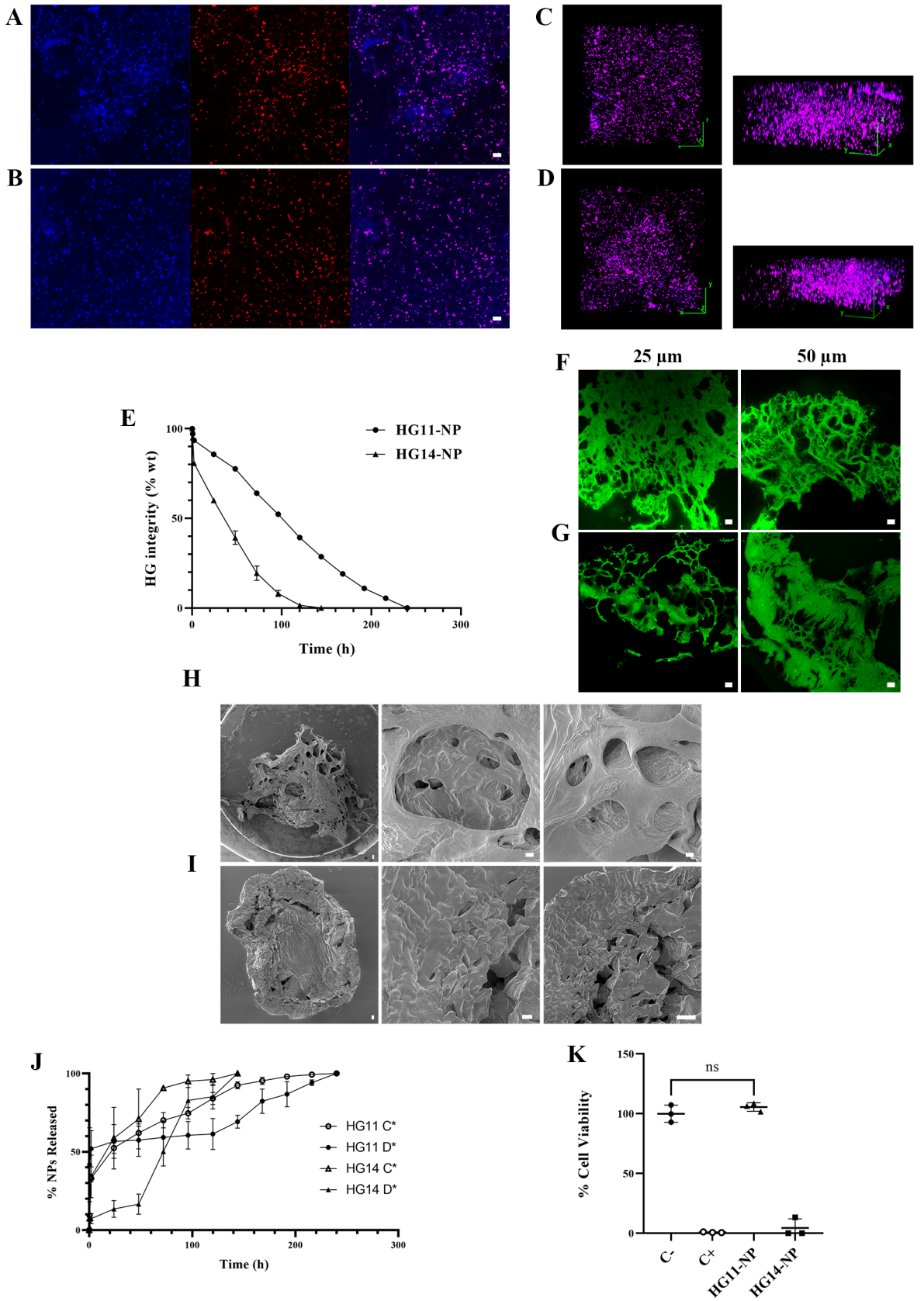

Figure 5. (A) Confocal microscopy images of C6RH polyplexes loaded into hydrogel HG11 (cy5-tagged pBAE shell: blue channel; cy3-tagged DNA core: red channel. Purple results from the pBAE and DNA signal overlap). (B) Confocal microscopy images of C6RH polyplexes loaded into hydrogel HG14 (same tags and channels than that used in A). Scale bar for A and B: 100 μm. (C) Three-dimensional construction of a 79 μm thick section of HG11 doped with C6RH-cy5 encapsulating pGFP-cy3. (D) Three-dimensional construction of a 57 μm thickness section of HG14 doped with C6RH-cy5 encapsulating pGFP-cy3. E) Degradation of hydrogels HG11 and HG14 loaded with polyplexes was tracked using

https://doi.org/10.1021/acsbiomaterials.1c00159
ACS Biomater. Sci. Eng. XXXX, XXX, XXX−XXX

Figure 5. continued

fluorescently labeled pBAE, which was converted to weight percent of pBAE in the hydrogel as a measure of hydrogel integrity; n = 2. (F, G) Confocal microscopy images of 25 and 50 μm slices of FITC-tagged C6RH-loaded HG11 and HG14, respectively. Scale bar for F and G: 50 μm. (H, I) SEM images of lyophilized bulk C6RH-loaded hydrogels HG11 and HG14, respectively; scale bar: 50 μm. (J) Release of fluorescently labeled C6RH nanoparticles from the hydrogels HG11 and HG14. C* corresponds to nanoparticles with cy3-tagged pBAE (shell) and D* to nanoparticles with cy3-tagged DNA (core); n = 2. (K) Cytotoxicity (in % cell viability) of C6RH-loaded HG11 and HG14 after 24 h of transfection.

swelling ratio was not affected by the differences in PEG-pBAE ratio (Figure S7), suggesting that both samples have similar cross-linking density and pore size. Fluorescence microscopy (Figures 4B−F) showed average pore sizes of 17.9 and 17.6 μm for HG11 and HG14, respectively (Figure S8). These data correlate with the similar swelling ratios and confirms that the cross-linking density (overall number of chemical bonds) is statistically similar for both formulations, as the ratio between chemical groups is maintained constant (SH:SSPy ratios of 2:1 for HG11 and 1:2 for HG14). It is important to highlight, though, that although the average cross-linking density may be statistically similar, the pore size distribution shows striking differences, with HG11 presenting a lower distribution of pore sizes ranging between 5 and 100 μm, while the pore size of HG14 ranges from 1 to almost 1000 μm (Figure S8). While there is no difference in swelling ratio between both formulations for a given drying protocol (oven or lyophilization), the drying method itself has a considerable influence on the swelling ratio, with an approximately 400% increase when the hydrogel is lyophilized compared to oven-dried (Figure S7). Lyophilization can extract water more efficiently than drying at 37 °C, as well as the DMSO used as the stock solutions solvent, hence leading to larger increases in reswelling ratios.

Rheological studies revealed that the storage moduli (G') for both formulations were higher than the loss moduli (G''), indicating that these hydrogels store energy elastically and hence behave as viscoelastic gels. Interestingly, despite both formulations having similar swelling ratios and cross-linking density, they showed stark differences in their behavior under deformation. HG11 formulation shows a linear viscoelastic region at low strain percentages not observed in HG14 formulation, with G' being independent of the applied deformation. As the percentage of strain increases, G' of HG11 slowly decreases as the network gradually deforms and the polymeric chains rearrange to minimize the effect of the stress applied (Figure 4G). In comparison, G' values of HG14 do not show a clear linear viscoelastic region. Hence, the G' decreases gradually (Figure 4H), suggesting the development of microfractures. This behavior is likely due to the large pores observed in fluorescence microscopy, facilitating points of increased stress levels that enabled fractures to be created and propagated. As a result, the energy that can be stored elastically (G') falls drastically during these events, making these hydrogels more brittle and likely to break during mechanical deformation. This conclusion was further confirmed when studying the lyophilized hydrogels by SEM, where HG11 can resist the lyophilization process, in contrast to HG14 that exhibits several internal fractures (Figures 4I−J). Hence, the HG14 formulation is more brittle than HG11.

Degradation and Cytotoxicity of PEG:pBAE Hydrogels. Hydrogel degradation was tracked using fluorescence, with the integrity of the hydrogel plotted as the ratio of the remaining fluorescence to the total initial fluorescence (Figure 4K). HG14 completely degraded after roughly 15 days, compared to 8 days for HG11. The burst release was more pronounced in the HG11 formulation than to the HG14 (37% burst release in HG11 compared to 15% for HG14). This seemingly contradicts our previous data reporting both formulations having the same average pore size, in which case a similar degradation profile would be expected. However, HG14 median pore size is smaller than that of HG11, suggesting that even though there are a few large pores and cracks in the biomaterial, the majority of the pores are indeed smaller than in the HG11 formulation (7.6 μm for HG14 compared to 16.9 μm for HG11) This supports the slower degradation observed initially, as well as the rapid disintegration of the hydrogel after a few days, when it breaks into macroscopic pieces because of the effect of the larger pores.

We next assessed the viability of HDFs in contact with hydrogel degradation byproducts released at different time intervals (0−24 h, 24−72 h, and 72−168 h). The starting reagents used to form the hydrogels (pBAE and 4-arm PEG) were also dissolved separately in culture medium at the concentration used for the hydrogel preparation. Cell viability experiments showed no significant cytotoxicity from the degradation byproducts of HG11 collected after 24, 72, or 168 h (Figure 4L, triangles). By contrast, HG14 degradation byproducts released in the first 24 h caused approximately 75% HDF toxicity, whereas no toxicity was observed when cells were exposed to degradation products released after 24 h (Figure 4L, squares). It is important to highlight that cells exposed to degradation byproducts at 72 h included only byproducts from the 24−72-h window, but not the initial 0−24 h window byproducts, and the same applies for the time point at 168 h, which contained only the 72−168 h byproducts. Hence, the behavior observed suggests that the initial burst release from HG14 leads to a high enough concentration of byproducts in the media to elicit fibroblast toxicity. Even though we reported lower burst release for HG14 compared to HG11 in relative numbers (% pBAE released of total pBAE), HG14 contains 4-fold higher pBAE content than HG11, leading to overall higher concentration of byproducts in the media after the initial burst release, causing higher toxicity. Indeed, the toxicity of the individual hydrogel components revealed that, while PEG-SH causes no significant cell death compared to the negative control, pBAEs are toxic at high concentrations (Figure 4L, white dots). Altogether, the data support the hypothesis that the burst release of pBAE polymers from HG14 is toxic to dermal fibroblasts, whereas HG11 shows no significant toxicity, hence making this formulation more suited for use as a dermal wound dressing for the release of therapeutics.

Characterization of C6RH-loaded composite hydrogels. C6RH nanoparticles were incorporated into both hydrogel formulations (HG11 and HG14) to attain sustained local release and prolonged HDFs transfection. First, we studied the stability and distribution of nanoparticles within

https://doi.org/10.1021/acsbiomaterials.1c00159
ACS Biomater. Sci. Eng. XXXX, XXX, XXX−XXX

the hydrogel via confocal microscopy, where 2% of C6RH polymer and 10% of pGFP were tagged with cy5 and cy3, respectively. Fluorescence colocalization was used as a surrogate measurement of particle stability, revealing that tagged C6RH (blue) and pGFP (red) colocalized with a Pearson's *R* value of 0.97 and 0.90 (Figures 5A, B for HG11 and HG14, respectively). Manders' overlap coefficient, more accurate for images with different intensities,[61,62] also revealed high colocalization of the fluorescent signals (HG11-NP: 0.91 and 1.00; HG14-NP: 0.98 and 0.84 for channels 1 and 2, respectively). High colocalization of C6RH polymers and plasmid indicates that the nanoparticles formed are stable within the hydrogel structure, meaning they do not degrade or become undone through electrostatic interactions with PBAEs in the hydrogel). Three-dimensional rendering of the hydrogel images showed that polyplexes were homogeneously distributed throughout the volume of the hydrogel in both HG11 (Figure 5C) and HG14 (Figure 5D) formulations.

Kinetics of pBAE Polyplexes Release from the Hydrogels. Fluorescein-labeled HG11 and HG14 loaded with pBAE polyplexes (HG11-NP and HG14-NP) were prepared and degradation experiments were performed as described above. The release of polyplexes was also fluorescently tracked by labeling either the C6RH polymer shell or the encapsulated pGFP with cy3 at concentrations of 1 and 10%, respectively. The addition of nanoparticles had a different impact on the overall degradation profiles of both formulations. Although complete degradation of HG11-NP occurred over a longer time-scale than that of HG11 (240 h for HG11-NP versus 200 h for HG11), HG14-NP degraded completely in almost a third of the time in comparison to HG14 (144 h compared to 360 h, Figure 5E). Interestingly, the addition of nanoparticles to the HG11 formulation leads to the elimination of the initial burst release and a close to zero-order degradation kinetics. To eliminate a dilution factor as the cause of the unexpected behavior of HG14, we studied the degradation of new formulations with equal final volumes (referred as HG14−500v and HG14−500v-NP). Despite having different final volumes (and hence reactants concentrations), HG14−500v presented similar degradation profile than HG14 (Figure S9), suggesting that the unexpected degradation kinetics were not caused by a dilution factor when adding the nanoparticles.

We then tested the effect of adding polyplexes to these new formulations (maintaining the final volume fixed). The data revealed the same unexpected acceleration of release kinetics previously observed in HG14-NP samples. Hence, the unexpected behavior of HG14-NP is not due to a dilution factor caused by the addition of nanoparticles solution to the hydrogel mix but rather to the nanoparticles themselves interacting unexpectedly with the hydrogel network. We also explored whether decreasing the concentration of nanoparticles by half could restore the degradation profile of HG14−500v. Once again, the degradation kinetics of this sample were accelerated compared to the hydrogel formulation without nanoparticles, and followed similar profile than that containing double the amount of polyplexes. Given that this phenomenon is not observed in HG11-NP (containing 4-fold less molar ratio of pBAE), it is reasonable to hypothesize that the interactions of the excess of $C32T_2CR3$ pBAE in the hydrogel with C6RH pBAE in the nanoparticles might be the cause of the hydrogel network destabilization and enhanced degradation kinetics. Indeed, both HG14-NP and HG14−500v-NP experienced visible macroscopic holes and started to break into pieces after 48 h, leading to an acceleration of the degradation. This also correlates with the increased fragility of HG14 formulation from our rheological studies. Fluorescence microscopy analysis of cryosectioned HG14-NP samples also revealed pores are not distributed in a uniform manner but forming cracks through the hydrogel (Figure 5G), as opposed to the more uniform pore size distribution of HG11-NP samples (Figure 5F and Figure S10). SEM image analysis of whole, lyophilized hydrogels corroborated these findings and confirmed that the observed cracks and large pores were not artifacts of the mechanical cryosectioning process (Figure 5H, I).

The unexpected behavior of HG14-NP formulation was also observed in the polyplex release experiments. Both C6RH forming the nanoparticle shell and encapsulated DNA were released following similar kinetics from HG11-NP samples (Figure 5J, circles), suggesting that the initial nanoparticle stability observed in confocal microscopy is maintained over time and after delivery. Contrarily, most of the C6RH pBAE forming the nanoparticles loaded in HG41-NP was quickly and steadily released within 72 h, whereas the DNA remained within the hydrogel for the first 48 h, and then was quickly released in the following 48 h (Figure 5J, triangles). This points toward polyplexes' disruption after hydrogel formation, followed by quick release of C6RH owing to electrostatic repulsion with $C32T_2CR3$ polymers forming the hydrogel network. Negatively charged DNA can then interact with positively charged $C32T_2CR3$ hydrogel network and be released with the bulk material as it fractures after 48 h. This indicates that, as inferred above from the degradation data, high $C32T_2CR3$ concentrations can interact adversely with C6RH polymers, leading to the destabilization of both the hydrogel network and the nanoparticles structure. Further research, beyond the scope of this manuscript, is needed to confirm our hypothesis that the underlying mechanism is based on the repulsive forces between positively charged polymers.

Before quantifying the transfection efficiency of mRNA-loaded polyplexes released from the hydrogel formulations in HDFs, a cytotoxicity assay of the composite material in direct contact with cells was performed. The viability of fibroblasts treated with the formulation HG11 did not show any significant difference compared to untreated fibroblast (Figure 5K), consistent with previously conducted cytotoxicity studies using the hydrogel's degradation products (without polyplexes). In contrast, cells treated with the formulation HG14-NP presented a cell viability comparable to that of the positive control, revealing again that the increase of pBAE in the formulation causes high cytotoxicity. The nontoxic formulation HG11-NP was then compared with a control consisting of formulation HG11 loaded with polyplexes formed with the commercially available positive control Polyplus JetMESSENGER. The incorporation of these new polyplexes encapsulating the same amount of mRNA as the the pBAE nanoparticles resulted in the hydrogel's structure disruption, thus making the hydrogel completely degrade within a few hours and leading to higher cytotoxicity (Figure S11).

Transfection Efficiency of Hydrogels Doped with mRNA-GFP-Loaded C6RH Polyplexes in HDFs. According to the data obtained in the release experiments, HG11-NP and HG14-NP hydrogels were doped with the necessary amount of polyplexes to release the same quantity of mRNA-GFP per cell when compared to the transfection experiments after 24 h

https://doi.org/10.1021/acsbiomaterials.1c00159
ACS Biomater. Sci. Eng. XXXX, XXX, XXX−XXX

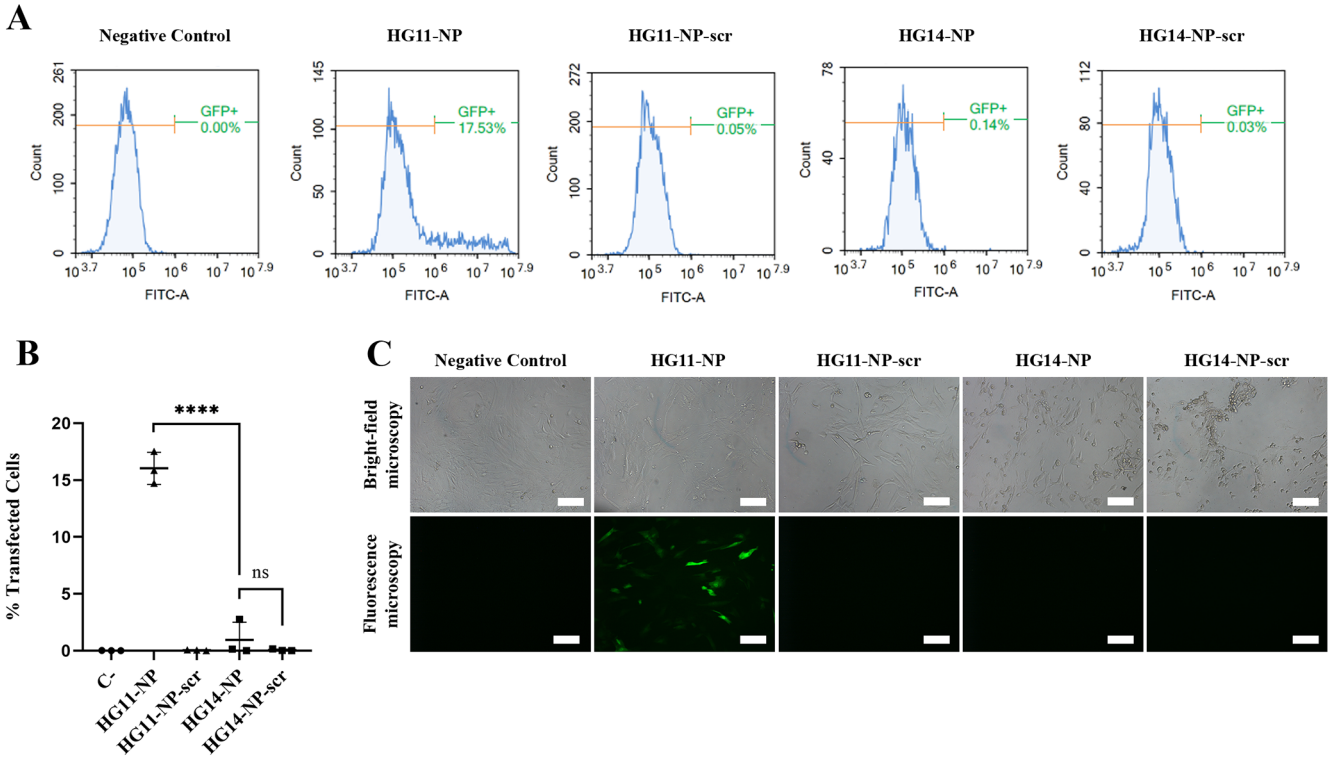

Figure 6. (A) FACS graphs showing the percentage of single HDF cells counted expressing GFP after transfection using the C6RH-loaded polyplexes encapsulating mRNA-GFP or a scrambled RNA. (B) Percentage of transfected cells after 24 h. HDFs were seeded on 48-well plates and the hydrogel formulations studied were placed on top of the cells. (C) Bright-field and fluorescence microscopy images of HDFs after 24 h contact with the hydrogel formulations used in the transfection experiment. Scale bar: 100 μm. $n = 3$. *$p < 0.05$; **$p < 0.01$; ***$p < 0.001$; ****$p < 0.0001$.

transfection (Figure 5J). A scrambled mRNA sequence encapsulated in C6RH and loaded into both hydrogel formulations served as negative controls, as well as non-transfected cells. HG11-NP formulation showed a significant difference in mRNA-GFP transfection compared to the same formulation encapsulating scrambled RNA as genetic material, with roughly 20% of HDF expressing GFP (Figure 6A, B). The transfection efficiency is lower than that observed when we incubate cells with free nanoparticles (without hydrogel release system). This is to be expected given that cells are exposed to a lower nanoparticle concentration throughout the experiment owing to the sustained release. At the time of fluorescence measurement, not all released nanoparticles have been uptaken by cells and not all uptaken nanoparticles have been translated into green fluorescence protein. Moreover, previous studies report that GFP protein expression progressively increases in the 24 h following mRNA transfection, and that there is an inherently large cell-to-cell variability in the expression levels of GFP of transfected cells.[63] Hence, only those cells transfected in the first few hours are expected to emit a significant amount of fluorescence at the time of measurement. The polyplexes formed by the commercially available Polyplus JetMESSENGER were also loaded into the formulation HG11 and the hydrogel formed was used as a control to transfect HDFs in the same way, but no transfection was observed (Figure S12).

Interestingly, the green fluorescence expression of HDFs transfected with GFP-mRNA-loaded HG14-NP was not significantly different from that of the same hydrogel loaded with scrambled mRNA, indicating that no transfection takes place with these formulations (Figure 6A, B). This aligns with the data gathered in the release experiments, where the genetic material and the C6RH polymer forming the polyplexes were released with different kinetics, and supports our hypothesis that polyplexes loaded into HG14 hydrogels degrade after a few hours, rendering them nonfunctional as transfection reagents. Hence, the formulation we herein name HG11-NP shows the capability to transfect primary dermal cells with a relatively high efficiency without compromising cell viability, and hence has high potential as an injectable wound dressing for gene therapy of chronic and delayed-healing wounds.

CONCLUSIONS

Gene therapy is rapidly gaining traction in our society, especially with the recent approval of mRNA vaccines. There is a pressing need for new and improved transfection reagents along with suitable delivery vehicles that can be easily translated into clinical therapeutic approaches to deliver genetic material to all types of cells. Although a significant effort has been placed into developing nanotechnology for the transfection of tumor cells, the viable and efficacious options for primary human cells are limited. Cutaneous chronic wounds display altered gene expression and mRNA dysregulation and could benefit from gene therapy. However, their irregular topology often makes it difficult to deliver any therapeutic in a sustained and controlled manner. In this work, we have developed a prototype of wound dressing based on a viscoelastic hydrogel made of poly(β-amino ester)s and PEG polymers. We have designed this wound dressing to be biodegradable, cytocompatible, and most importantly, injectable. The latter property allows the material to be applied in liquid form and gel in situ to adapt to irregular, deep wounds such as chronic ulcers. We have also shown that this novel

https://doi.org/10.1021/acsbiomaterials.1c00159
ACS Biomater. Sci. Eng. XXXX, XXX, XXX−XXX

hydrogel is suitable as a depot for controlled delivery of pBAE nanoparticles loaded with genetic material over a variable time frame (8−15 days depending on the formulation). As a proof of concept, the nanoparticles developed herein were shown to efficiently transfect human dermal fibroblasts with both mRNA and DNA encoding for green fluorescent protein. Particle stability and transfection efficiency were maintained after release from the hydrogel, demonstrating that this prototype wound dressing is an ideal candidate for gene therapy applied to cutaneous chronic wound healing. These results lay the groundwork for future studies exploring the therapeutic potential of the platform using preclinical models of defective wound healing. Further studies will aim at validating the transfection efficiency of these pBAE nanoparticles in other human primary cell types (i.e., endothelial cells, osteocytes, cardiomyocytes) to generalize the use of this platform for improving impaired healing or simply accelerating normal healing after surgery or trauma, in turn reducing the length of hospitalization and accelerating the return to work.

■ ASSOCIATED CONTENT

Supporting Information

The Supporting Information is available free of charge at https://pubs.acs.org/doi/10.1021/acsbiomaterials.1c00159.

Figure S1, characterization of polymer $C32T_2$ by ^1H NMR; Figure S2, characterization of polymer $C32T_2CR3$ by ^1H NMR; Figure S3, size and zeta potential graphs obtained by DLS; Table S1, nanoparticle hydrodynamic diameter and PdI of the formulations studied; Figure S4, transfection efficiency using GFP-coding polynucleotides; Figure S5, transfection efficiency using luciferase-coding polynucleotides; Figure S6, evidence on hydrogel formation via disulfide coupling by ^1H NMR; Figure S7, swelling ratios of the hydrogel formulations studied. Figure S8, pore size distribution in HG11 and HG14; Figure S9, degradation of hydrogels HG14 and HG14−500v; Figure S10, pore size distribution in formulations HG11, HG14, HG11-NP, and HG14-NP; Figure S11, cell viability of HDFs after transfection using C6RH nanoparticles and Polyplus JetMESSENGER as positive control; Figure S12, transfection of HDFs using C6RH nanoparticles and Polyplus JetMESSENGER as positive control (PDF)

■ AUTHOR INFORMATION

Corresponding Authors

Salvador Borrós − *Grup d'Enginyeria de Materials (GEMAT), Institut Químic de Sarrià, Universitat Ramon Llull, Barcelona 08017, Spain;* orcid.org/0000-0002-4003-0381; Email: salvador.borros@iqs.url.edu

Nuria Oliva − *Department of Bioengineering, Imperial College London, London SW7 2AZ, United Kingdom;* orcid.org/0000-0002-6305-0801; Email: n.oliva-jorge@imperial.ac.uk

Authors

Jose Antonio Duran Mota − *Grup d'Enginyeria de Materials (GEMAT), Institut Químic de Sarrià, Universitat Ramon Llull, Barcelona 08017, Spain; Department of Bioengineering, Imperial College London, London SW7 2AZ, United Kingdom*

Júlia Quintanas Yani − *Grup d'Enginyeria de Materials (GEMAT), Institut Químic de Sarrià, Universitat Ramon Llull, Barcelona 08017, Spain; Department of Bioengineering, Imperial College London, London SW7 2AZ, United Kingdom*

Benjamin D. Almquist − *Department of Bioengineering, Imperial College London, London SW7 2AZ, United Kingdom;* orcid.org/0000-0001-9718-777X

Complete contact information is available at: https://pubs.acs.org/10.1021/acsbiomaterials.1c00159

Author Contributions

S.B. and N.O. conceived the project and designed the experiments. J.A.D.M. and J.Q.Y. designed and performed the experiments and collected and analyzed the data. B.D.A. provided mentorship and advice. B.D.A., S.B., and N.O. secured the funding for the research. J.A.D.M., S.B., and N.O. cowrote the manuscript. All authors analyzed and discussed the results and reviewed the manuscript. All authors approved the final version of the manuscript.

Notes

The authors declare no competing financial interest.

■ ACKNOWLEDGMENTS

N.O. acknowledges funding from the European Union's Horizon 2020 research and innovation programme under the Marie Sklodowska-Curie grant agreement 712949 (TECNIOspring PLUS) and from the Agency for Business Competitiveness of the Government of Catalonia, along with funding from an Imperial College Research Fellowship and a British Skin Foundation Small Grant Award 005/BSFSG/20. S.B. acknowledges funding from the Ministerio de Ciencia, Innovación y Universidades, project RTI2018-094734-B-C22. B.D.A acknowledges funding from the Engineering and Physical Sciences Research Council, project EP/R041628/1. We thank Dr. Meysam Keshavarz from the Hamlyn Centre at Imperial College London for assistance with SEM imaging, Jessica Rowley and Larissa Zarate-Garcia from the SAFB Flow Cytometry Core Facility for their assistance with the cytometer, and Miguel Hermida Ayala from the Department of Bioengineering at Imperial College London and Cristina Fornaguera Puigvert from the Department of Bioengineering at Institut Químic de Sarrià for assistance with confocal microscopy imaging. We also want to thank Núria Agulló Chaler for her knowledge and assistance with the rheometry experiments and Marta Guerra Rebollo for assistance with the luciferase mRNA transfection experiments.

■ ABBREVIATIONS

4arm-PEG-SH, thiolated 4arm-polyethylene glycol; FACS, fluorescence-activated cell sorting; HDFs, human dermal fibroblasts; OM-pBAEs, oligopeptide-modified poly(β-amino esters)s; pBAEs, poly(β-amino esters)s; SPDP, 3-(2-pyridyldithio)propanoic acid

■ REFERENCES

(1) Werner, S.; Grose, R. Regulation of Wound Healing by Growth Factors and Cytokines. *Physiol. Rev.* **2003**, *83* (3), 835−870.

(2) Singer, A. J.; Clark, R. A. F. Cutaneous Wound Healing. *N. Engl. J. Med.* **1999**, *341* (10), 738−746.

(3) Guo, S.; DiPietro, L. A. Factors Affecting Wound Healing. *J. Dent. Res.* **2010**, *89* (3), 219−229.

(4) Sen, C. K. Human Wounds and Its Burden: An Updated Compendium of Estimates. *Adv. Wound Care* **2019**, *8* (2), 39−48.
(5) Eming, S. A.; Martin, P.; Tomic-Canic, M. Wound Repair and Regeneration: Mechanisms, Signaling, and Translation. *Sci. Transl. Med.* **2014**, *6* (265), 265sr6.
(6) Broughton, G.; Janis, J. E.; Attinger, C. E. Wound Healing: An Overview. *Plast. Reconstr. Surg.* **2006**, *117*, 1e−32e.
(7) Morton, L. M.; Phillips, T. J. Wound Healing and Treating Wounds. *J. Am. Acad. Dermatol.* **2016**, *74* (4), 589−605.
(8) Han, G.; Ceilley, R. Chronic Wound Healing: A Review of Current Management and Treatments. *Adv. Ther.* **2017**, *34* (3), 599−610.
(9) van de Vyver, M.; Niesler, C.; Myburgh, K. H.; Ferris, W. F. Delayed Wound Healing and Dysregulation of IL6/STAT3 Signalling in MSCs Derived from Pre-Diabetic Obese Mice. *Mol. Cell. Endocrinol.* **2016**, *426*, 1−10.
(10) Takematsu, E.; Spencer, A.; Auster, J.; Chen, P.-C.; Graham, A.; Martin, P.; Baker, A. B. Genome Wide Analysis of Gene Expression Changes in Skin from Patients with Type 2 Diabetes. *PLoS One* **2020**, *15* (2), No. e0225267.
(11) Layliev, J.; Wilson, S.; Warren, S. M.; Saadeh, P. B. Improving Wound Healing with Topical Gene Therapy. *Adv. Wound Care* **2012**, *1* (5), 218−223.
(12) Oryan, A.; Alemzadeh, E.; Zarei, M. Basic Concepts, Current Evidence, and Future Potential for Gene Therapy in Managing Cutaneous Wounds. *Biotechnol. Lett.* **2019**, *41* (8−9), 889−898.
(13) Khalil, A. S.; Yu, X.; Umhoefer, J. M.; Chamberlain, C. S.; Wildenauer, L. A.; Diarra, G. M.; Hacker, T. A.; Murphy, W. L. Single-Dose MRNA Therapy via Biomaterial-Mediated Sequestration of Overexpressed Proteins. *Sci. Adv.* **2020**, *6* (27), No. eaba2422.
(14) Sun, N.; Ning, B.; Hansson, K. M.; Bruce, A. C.; Seaman, S. A.; Zhang, C.; Rikard, M.; DeRosa, C. A.; Fraser, C. L.; Wågberg, M.; Fritsche-Danielson, R.; Wikström, J.; Chien, K. R.; Lundahl, A.; Hölttä, M.; Carlsson, L. G.; Peirce, S. M.; Hu, S. Modified VEGF-A MRNA Induces Sustained Multifaceted Microvascular Response and Accelerates Diabetic Wound Healing. *Sci. Rep.* **2018**, *8* (1), 17509−17519.
(15) Khalil, I. A.; Sato, Y.; Harashima, H. Recent Advances in the Targeting of Systemically Administered Non-Viral Gene Delivery Systems. *Expert Opin. Drug Delivery* **2019**, *16* (10), 1037−1050.
(16) Nayerossadat, N.; Ali, P.; Maedeh, T. Viral and Nonviral Delivery Systems for Gene Delivery. *Adv. Biomed. Res.* **2012**, *1* (2), 27−37.
(17) Hirsch, T.; Spielmann, M.; Yao, F.; Eriksson, E. Gene Therapy in Cutaneous Wound Healing. *Front. Biosci., Landmark Ed.* **2007**, *12* (7), 2507−2518.
(18) Wu, P.; Chen, H.; Jin, R.; Weng, T.; Ho, J. K.; You, C.; Zhang, L.; Wang, X.; Han, C. Non-Viral Gene Delivery Systems for Tissue Repair and Regeneration. *J. Transl. Med.* **2018**, *16* (1), 29−48.
(19) Aggarwal, R.; Targhotra, M.; Kumar, B.; Sahoo, P.; Chauhan, M. K. Polyplex: A Promising Gene Delivery System. *Int. J. Pharm. Sci. Nanotechnol.* **2019**, *12* (6), 4681−4686.
(20) Kozielski, K. L.; Tzeng, S. Y.; Hurtado De Mendoza, B. A.; Green, J. J. Bioreducible Cationic Polymer-Based Nanoparticles for Efficient and Environmentally Triggered Cytoplasmic SiRNA Delivery to Primary Human Brain Cancer Cells. *ACS Nano* **2014**, *8* (4), 3232−3241.
(21) Segovia, N.; Dosta, P.; Cascante, A.; Ramos, V.; Borrós, S. Oligopeptide-Terminated Poly(ß-Amino Ester)s for Highly Efficient Gene Delivery and Intracellular Localization. *Acta Biomater.* **2014**, *10* (5), 2147−2158.
(22) Tzeng, S. Y.; Hung, B. P.; Grayson, W. L.; Green, J. J. Cystamine-Terminated Poly(Beta-Amino Ester)s for SiRNA Delivery to Human Mesenchymal Stem Cells and Enhancement of Osteogenic Differentiation. *Biomaterials* **2012**, *33* (32), 8142−8151.
(23) Tzeng, S. Y.; Green, J. J. Subtle Changes to Polymer Structure and Degradation Mechanism Enable Highly Effective Nanoparticles for SiRNA and DNA Delivery to Human Brain Cancer. *Adv. Healthcare Mater.* **2013**, *2* (3), 468−480.
(24) Zugates, G. T.; Peng, W.; Zumbuehl, A.; Jhunjhunwala, S.; Huang, Y. H.; Langer, R.; Sawicki, J. A.; Anderson, D. G. Rapid Optimization of Gene Delivery by Parallel End-Modification of Poly(β-Amino Ester)S. *Mol. Ther.* **2007**, *15* (7), 1306−1312.
(25) Ahmad, A.; Khan, J. M.; Haque, S. Strategies in the Design of Endosomolytic Agents for Facilitating Endosomal Escape in Nanoparticles. *Biochimie* **2019**, *160*, 61−75.
(26) Keeney, M.; Ong, S. G.; Padilla, A.; Yao, Z.; Goodman, S.; Wu, J. C.; Yang, F. Development of Poly(β-Amino Ester)-Based Biodegradable Nanoparticles for Nonviral Delivery of Minicircle DNA. *ACS Nano* **2013**, *7* (8), 7241−7250.
(27) Dosta, P.; Ramos, V.; Borrós, S. Stable and Efficient Generation of Poly(β-Amino Ester)s for RNAi Delivery. *Mol. Syst. Des. Eng.* **2018**, *3* (4), 677−689.
(28) Meenach, S. A.; Otu, C. G.; Anderson, K. W.; Hilt, J. Z. Controlled Synergistic Delivery of Paclitaxel and Heat from Poly(β-Amino Ester)/Iron Oxide-Based Hydrogel Nanocomposites. *Int. J. Pharm.* **2012**, *427* (2), 177−184.
(29) Perni, S.; Prokopovich, P. Poly-Beta-Amino-Esters Nano-Vehicles Based Drug Delivery System for Cartilage. *Nanomedicine* **2017**, *13* (2), 539−548.
(30) Tzeng, S. Y.; Guerrero-Cázares, H.; Martinez, E. E.; Sunshine, J. C.; Quiñones-Hinojosa, A.; Green, J. J. Non-Viral Gene Delivery Nanoparticles Based on Poly(β-Amino Esters) for Treatment of Glioblastoma. *Biomaterials* **2011**, *32* (23), 5402−5410.
(31) Segovia, N.; Pont, M.; Oliva, N.; Ramos, V.; Borrós, S.; Artzi, N. Hydrogel Doped with Nanoparticles for Local Sustained Release of SiRNA in Breast Cancer. *Adv. Healthcare Mater.* **2015**, *4* (2), 271−280.
(32) Dickens, S.; Van den Berge, S.; Hendrickx, B.; Verdonck, K.; Luttun, A.; Vranckx, J. J. Nonviral Transfection Strategies for Keratinocytes, Fibroblasts, and Endothelial Progenitor Cells for Ex Vivo Gene Transfer to Skin Wounds. *Tissue Eng., Part C* **2010**, *16* (6), 1601−1608.
(33) Paidikondala, M.; Kadekar, S.; Varghese, O. Innovative Strategy for 3D Transfection of Primary Human Stem Cells with BMP-2 Expressing Plasmid DNA: A Clinically Translatable Strategy for Ex Vivo Gene Therapy. *Int. J. Mol. Sci.* **2019**, *20* (1), 56−68.
(34) Gresch, O.; Altrogge, L. Transfection of Difficult-to-Transfect Primary Mammalian Cells. In *Protein Expression in Mammalian Cells: Methods and Protocols*; Hartley, J. L., Ed.; Methods in Molecular Biology; Springer Science+Business Media, 2012; Vol. *801*, pp 65−74.
(35) Koster, J.; Waterham, H. R. Transfection of Primary Human Skin Fibroblasts for Peroxisomal Studies. In *Peroxisomes: Methods and Protocols*; Schrader, M., Ed.; Methods in Molecular Biology; Springer Science+Business Media, 2017; Vol. *1595*, pp 63−67.
(36) Fliervoet, L. A. L.; Engbersen, J. F. J.; Schiffelers, R. M.; Hennink, W. E.; Vermonden, T. Polymers and Hydrogels for Local Nucleic Acid Delivery. *J. Mater. Chem. B* **2018**, *6* (36), 5651−5670.
(37) Oliva, N.; Conde, J.; Wang, K.; Artzi, N. Designing Hydrogels for On-Demand Therapy. *Acc. Chem. Res.* **2017**, *50* (4), 669−679.
(38) Boateng, J. S.; Matthews, K. H.; Stevens, H. N. E.; Eccleston, G. M. Wound Healing Dressings and Drug Delivery Systems: A Review. *J. Pharm. Sci.* **2008**, *97* (8), 2892−2923.
(39) Oliva, N.; Almquist, B. D. Spatiotemporal Delivery of Bioactive Molecules for Wound Healing Using Stimuli-Responsive Biomaterials. *Adv. Drug Delivery Rev.* **2020**, *161−162*, 22−41.
(40) Jones, A.; Vaughan, D. Hydrogel Dressings in the Management of a Variety of Wound Types: A Review. *J. Orthop. Nurs.* **2005**, *9*, S1−S11.
(41) Koehler, J.; Brandl, F. P.; Goepferich, A. M. Hydrogel Wound Dressings for Bioactive Treatment of Acute and Chronic Wounds. *Eur. Polym. J.* **2018**, *100*, 1−11.
(42) Kamoun, E. A.; Kenawy, E. R. S.; Chen, X. A Review on Polymeric Hydrogel Membranes for Wound Dressing Applications: PVA-Based Hydrogel Dressings. *J. Adv. Res.* **2017**, *8* (3), 217−233.
(43) Sharman, D. Moist Wound Healing: A Review of Evidence, Application and Outcome. *Diabet. Foot J.* **2003**, *6* (3), 112−116.

https://doi.org/10.1021/acsbiomaterials.1c00159
ACS Biomater. Sci. Eng. XXXX, XXX, XXX−XXX

(44) Sen, C. K. Wound Healing Essentials: Let There Be Oxygen. *Wound Repair Regen.* **2009**, *17* (1), 1−18.
(45) Cascone, S.; Lamberti, G. Hydrogel-Based Commercial Products for Biomedical Applications: A Review. *Int. J. Pharm.* **2020**, *573*, 118803−118821.
(46) Schreml, S.; Szeimies, R.-M.; Prantl, L.; Landthaler, M.; Babilas, P. Wound Healing in the 21st Century. *J. Am. Acad. Dermatol.* **2010**, *63* (5), 866−881.
(47) Berberich, B.; Thriene, K.; Gretzmeier, C.; Kühl, T.; Bayer, H.; Athanasiou, I.; Rafei-Shamsabadi, D. A.; Bruckner-Tuderman, L.; Nyström, A.; Kiritsi, D.; Dengjel, J. Proteomic Profiling of Fibroblasts Isolated from Chronic Wounds Identifies Disease-Relevant Signaling Pathways. *J. Invest. Dermatol.* **2020**, *140* (11), 2280−2290.
(48) Darby, I. A.; Laverdet, B.; Bonté, F.; Desmoulière, A. Clinical, Cosmetic and Investigational Dermatology Dovepress Fibroblasts and Myofibroblasts in Wound Healing. *Clin., Cosmet. Invest. Dermatol.* **2014**, *4* (7), 301−311.
(49) Kim, B. C.; Kim, H. T.; Park, S. H.; Cha, J. S.; Yufit, T.; Kim, S. J.; Falanga, V. Fibroblasts from Chronic Wounds Show Altered TGF-β-Signaling and Decreased TGF-β Type II Receptor Expression. *J. Cell. Physiol.* **2003**, *195* (3), 331−336.
(50) Madhyastha, R.; Madhyastha, H.; Nakajima, Y.; Omura, S.; Maruyama, M. MicroRNA Signature in Diabetic Wound Healing: Promotive Role of MiR-21 in Fibroblast Migration. *Int. Wound J.* **2012**, *9* (4), 355−361.
(51) Fornaguera, C.; Guerra-Rebollo, M.; Ángel Lázaro, M.; Castells-Sala, C.; Meca-Cortés, O.; Ramos-Pérez, V.; Cascante, A.; Rubio, N.; Blanco, J.; Borrós, S. MRNA Delivery System for Targeting Antigen-Presenting Cells In Vivo. *Adv. Healthcare Mater.* **2018**, *7* (17), 1800335.
(52) Dosta, P.; Segovia, N.; Cascante, A.; Ramos, V.; Borrós, S. Surface Charge Tunability as a Powerful Strategy to Control Electrostatic Interaction for High Efficiency Silencing, Using Tailored Oligopeptide-Modified Poly(Beta-Amino Ester)s (PBAEs). *Acta Biomater.* **2015**, *20*, 82−93.
(53) Khalil, I. A.; Futaki, S.; Niwa, M.; Baba, Y.; Kaji, N.; Kamiya, H.; Harashima, H. Mechanism of Improved Gene Transfer by the N-Terminal Stearylation of Octaarginine: Enhanced Cellular Association by Hydrophobic Core Formation. *Gene Ther.* **2004**, *11* (7), 636−644.
(54) Takigawa, D. Y.; Tirrell, D. A. Disruption of Phospholipid Packing by Branched Poly(Ethylenimine) Derivatives. *Macromolecules* **1985**, *18* (3), 338−342.
(55) Rejman, J.; Oberle, V.; Zuhorn, I. S.; Hoekstra, D. Size-Dependent Internalization of Particles via the Pathways of Clathrin- and Caveolae-Mediated Endocytosis. *Biochem. J.* **2004**, *377* (1), 159−169.
(56) Prabha, S.; Zhou, W.-Z.; Panyam, J.; Labhasetwar, V. Size-Dependency of Nanoparticle-Mediated Gene Transfection: Studies with Fractionated Nanoparticles. *Int. J. Pharm.* **2002**, *244* (1−2), 105−115.
(57) Singh, R.; Lillard, J. W. Nanoparticle-Based Targeted Drug Delivery. *Exp. Mol. Pathol.* **2009**, *86* (3), 215−223.
(58) Kulkarni, S. A.; Feng, S. S. Effects of Particle Size and Surface Modification on Cellular Uptake and Biodistribution of Polymeric Nanoparticles for Drug Delivery. *Pharm. Res.* **2013**, *30* (10), 2512−2522.
(59) Faraji, A. H.; Wipf, P. Nanoparticles in Cellular Drug Delivery. *Bioorg. Med. Chem.* **2009**, *17* (8), 2950−2962.
(60) de Barros, A.; Tsourkas, A.; Saboury, B.; Cardoso, V.; Alavi, A. Emerging Role of Radiolabeled Nanoparticles as an Effective Diagnostic Technique. *EJNMMI Res.* **2012**, *2* (1), 39−53.
(61) Adler, J.; Parmryd, I. Quantifying Colocalization by Correlation: The Pearson Correlation Coefficient Is Superior to the Mander's Overlap Coefficient. *Cytometry, Part A* **2010**, *77* (8), 733−742.
(62) Pike, J. A.; Styles, I. B.; Rappoport, J. Z.; Heath, J. K. Quantifying Receptor Trafficking and Colocalization with Confocal Microscopy. *Methods* **2017**, *115*, 42−54.
(63) Reiser, A.; Woschée, D.; Mehrotra, N.; Krzysztoń, R.; Strey, H. H.; Rädler, J. O. Correlation of MRNA Delivery Timing and Protein Expression in Lipid-Based Transfection. *Integr. Biol.* **2019**, *11* (9), 362−371.

https://doi.org/10.1021/acsbiomaterials.1c00159
ACS Biomater. Sci. Eng. XXXX, XXX, XXX−XXX